Electronic Supplementary Information

Narrowband Multi-Resonance Pure-Red Emitters by Enhanced Molecular Orbitals Delocalization for High-Performance OLEDs

Xiaowei Wang,† [a] Tao Hua,† *[a, b] Nengquan Li,[a] Guohao Chen,[a] Zhanxiang Chen,[a] Jingsheng Miao,[a] Xiaosong Cao,[a] Chuluo, Yang*[a]

[a] X. Wang, Dr. T. Hua, Dr. N. Li, G. Chen, Dr. Z. Chen, Dr. J. Miao, Dr. X. Cao, Prof. C. Yang

Shenzhen Key Laboratory of New Information Display and Storage Materials, College of Materials Science and Engineering

Shenzhen University

Shenzhen 518060, P. R. China E-mail: clyang@szu.edu.cn

[b] Dr. T. Hua

Institute of Technology for Future Industry, School of Science and Technology Instrument Application Engineering

Shenzhen Institute of Information Technology

Shenzhen, 518172, P. R. China. Email: taohua@sziit.edu.cn

†These authors contributed equally in this work.

Contents

General Information

Unless otherwise stated, all starting materials were obtained from commercial suppliers and were used without further purification. All the reaction solvents were purified by solvent purification system prior to use.

The ^{1}H and ^{13}C nuclear magnetic resonance (NMR) spectra were recorded in deuterated chloroform ($CDCl_3$) solution on Bruker NMR spectrometer with tetramethylsilane (TMS, δ 0.00) as the internal standard. The high-resolution mass spectrometry (HR-MS) of the compounds was conducted on a Thermo Scientific LTQ Orbitrap XL with an ESI ion source.

Quantum Chemical Calculations

All simulation calculations were carried out with Gaussian 09 program package. Density functional theory (DFT) calculations on the geometrical and electronic properties of the ground-state were performed based on B3LYP density functional method with the basis set 6-31G(d, p). Time-dependent DFT (TD-DFT) calculations were also carried out using the same method. Higher-level spin-component scaling second-order approximate coupled-cluster (SCS-CC2) calculations were performed using the MRCC Program with cc-PVDZ method.

Thermal and Electrochemical Characterization

Thermogravimetric analysis (TGA) was conducted using TGA-Q50 Instrument (TA Instruments, America) at a heating rate of 10 °C/min from 50 to 800 °C under a nitrogen flow environment. The thermal decomposition temperatures (T_d) were determined by the recorded temperature at 5% weight loss.

Cyclic voltammetry (CV) measurements were carried out on a CHI600 electrochemical analyzer (Chenhua, China) at room temperature, with a conventional three-electrode system, which consists of a glassy carbon as working electrode, a platinum wire as auxiliary electrode, and an Ag/AgCl standard electrode using as the reference electrode. 0.1 M tetrabutylammonium hexafluorophosphate (Bu_4NPF_6) was used as the supporting electrolyte, and ferrocene was added as a calibrant. The HOMO energy levels (E_{HOMO}) of the three compounds were calculated according to the formula: E_{HOMO} (eV) = $-[4.8 + (E_{1/2(ox/red)} - E_{1/2(Fc+/Fc)})]$ eV. The LUMO energy levels of three compounds were then deduced from the HOMO levels and the energy gap between HOMO and LUMO level (E_{LUMO} = E_{HOMO} - E_{g}).

Photophysical Characterization

The UV-vis absorption spectra were measured in toluene by Shimadzu UV-2600 spectrophotometer (Shimadzu, Japan) at room temperature with a concentration of $1*10^{-5}$ M. The room temperature fluorescence, low-temperature fluorescence and phosphorescence spectra were monitored on a Hitachi F-7100 fluorescence spectrophotometer. The transient PL decay curves were completed by FluoTime 300 (PicoQuant GmbH) with a Picosecond Pulsed UV-LASTER (LASTER375) as the excitation source. The PL quantum efficiencies (PLQY, Φ_{PL}s) were achieved on a Hamamatsu UV-NIR absolute PL quantum yield spectrometer (C13534, Hamamatsu Photonics) equipped with an integrating sphere purged with dry argon to maintain an inert atmosphere.

Single Crystal X-ray Crystallographic Data

X-ray single crystal data of **BCzBN** was identified on a Bruker D8 Venture diffractometer using MoK radiation (λ = 0.71073) source. The selected crystal was kept at 150.0 K during data collection. Using Olex2 the structure was solved with the ShelXT structure solution program using Intrinsic Phasing and refined with the ShelXL refinement package using Least Squares minimization. Selected crystal data and experimental details are listed below. All crystallographic information in CIF format have been deposited at the Cambridge Crystallographic Data Center (CCDC) under deposition number 2373696 for **BCzBN**, via www.ccdc.cam.ac.uk/data_request/cif.

Analysis of Rate Constants

The rate constants of radiative decay ($k_{\mathrm{r,S}}$) and nonradiative decay ($k_{\mathrm{nr,S}}$) from S_1 to S_0 states could be estimated using the following equations.

$$k_{\mathrm{r,S}} = \Phi_{\mathrm{p}} k_{\mathrm{p}} + \Phi_{\mathrm{d}} k_{\mathrm{d}} \approx \Phi_{\mathrm{p}} k_{\mathrm{p}} \quad \text{……………………………………………Eq.(1)}$$

$$k_{\mathrm{nr,S}} = \frac{1-\Phi_{\mathrm{PL}}}{\Phi_{\mathrm{PL}}} k_{\mathrm{r,S}} \quad \text{…………………………………………………Eq.(2)}$$

Where k_{p} and k_{d} represent the decay rate constants for prompt and delayed fluorescence, respectively, which are in reciprocal relationship with the decay time constants (τ_{p} and τ_{d}) experimentally determined from transient PL characteristics.

Device Fabrication and Measurement

The device fabrication was adopted the Proven Process in our previous work. The ITO coated glass substrates with a sheet resistance of 15 Ω square^{-1} were consecutively ultrasonicated with acetone/ethanol and dried with nitrogen gas flow, followed by 20 min ultraviolet light-ozone (UVO) treatment in a UV-ozone surface processor (PL16 series, Sen Lights Corporation). Then the sample was transferred to the deposition system. Both 8-hydroxyquinolinolato-lithium (Liq) as electron injection layer and aluminum (Al) as cathode layer were deposited by thermal evaporation at 5×10^{-5} Pa. The organic layers were deposited at the rates of 0.2-3 Å/s. After the organic film deposition, Liq and Al layer were deposited with rates of 0.1 and 3 Å/s, respectively. For all the OLEDs, the emitting areas were determined by the overlap of two electrodes as 0.09 cm^2. The as-fabricated devices were measured in ambient environment without any encapsulation. The current density-voltage-luminance (*J*-*V*-*L*), *L*-*EQE* curves and electroluminescence spectra were measured using a Keithley 2400 source meter and an absolute EQE measurement system (C9920-12, Hamamatsu Photonics, Japan).

Synthesis

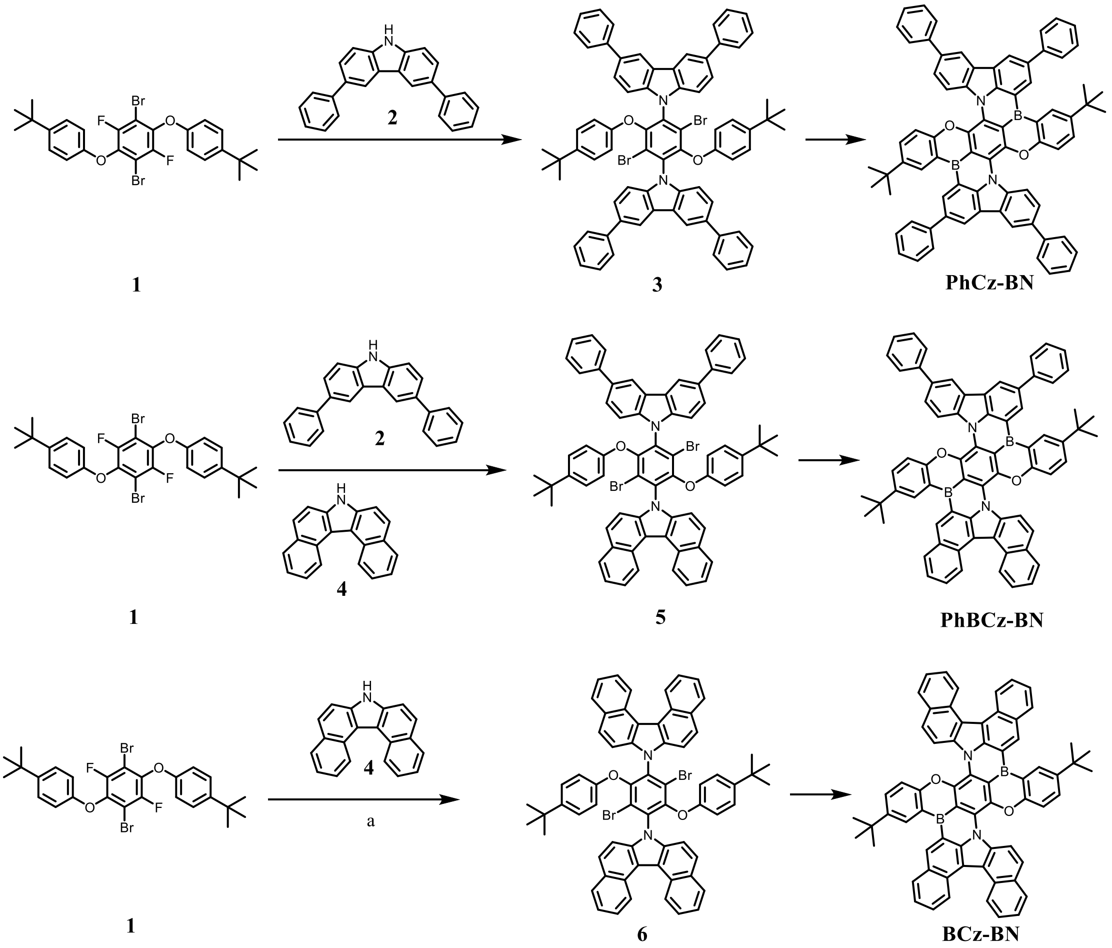

Scheme S1. The synthetic routes of **PhCzBN, PhBCzBN** and **BCzBN**.

Synthesis of 9,9'-(2,5-dibromo-3,6-bis(4-(tert-butyl)phenoxy)-1,4-phenylene)bis (3,6-diphenyl-9H-carbazole) (**3**)

Under argon atmosphere, compound **1** (2.8 g, 5 mmol), 3,6-diphenyl-9*H*-carbazole (3.5 g, 11 mmol) and Cs_2CO_3 (4.9 g, 15 mmol) were added into a two necked round bottom flask. Addition of DMF (30 mL) was added into the flask and the mixture was stirred for 12 hours at 80 °C. After cooling to room temperature, the mixture was poured into water and the crude product was obtained by filtration followed by washing with ethanol. Precursor **3** (5.8 g, 89%) was acquired as white solid. ^{1}H NMR (500 MHz, $CDCl_3$) δ 8.24 (s, 4H), 7.76–7.63 (m, 12H), 7.49 (t, *J* = 6.5 Hz, 8H), 7.36 (t, *J* = 7.0 Hz, 4H), 7.22 (d, *J* = 8.3 Hz, 4H), 6.74 (d, *J* = 9.0 Hz, 4H), 6.19 (d, *J* = 6.5 Hz, 4H), 0.95 (s, 18H). ^{13}C NMR (125 MHz, $CDCl_3$) δ 153.98, 150.76, 146.36, 141.79, 139.08, 134.13, 131.59, 128.83, 127.36, 126.72, 125.66, 125.38, 124.30, 121.43, 118.69, 115.09, 110.95, 33.91, 31.24.

Synthesis of **PhCzBN**

A solution of *t*-BuLi in hexane (1.3 M, 6 mmol) was added drop by drop to a solution of **3** (1.2 g, 1 mmol) in trimethylbenzene (30 mL) at 0 ºC under nitrogen atmosphere. After the mixture was stirred for 2 h at 60 °C, BBr_3 (0.85 mL, 9 mmol) was added slowly at 0 ºC. The reaction mixture was allowed to warm to room temperature and stirred for another 1 h. 2.0 mL N,N-diisopropylethylamine was added at 0 ºC, the reaction mixture was stirred at 140 ºC for 12 h. The reaction was cooled to room temperature, excess N,N-diisopropylethylamine (5.0 mL) was added into the mixture. Then the mixture was diluted with dichloromethane and washed with water for 3 times. The organic ingredients were dried over Na_2SO_4 for 15 min and removed by a rotatory evaporation. The crude product was purified by silica gel column chromatography, **PhCzBN** was recrystallized from CH_2Cl_2 and CH_3OH as a red solid (245 mg, 24%). ^1H NMR (500 MHz, $CDCl_3$) δ 8.52 (d, *J* = 1.5 Hz, 2H), 8.39 (d, *J* = 2.5 Hz, 2H), 8.28 (d, *J* = 1.5 Hz, 2H), 7.98 (d, *J* = 2.0 Hz, 2H), 7.63 (d, *J* = 7.0 Hz, 4H), 7.52 (d, *J* = 7.0 Hz, 4H), 7.44 – 7.36 (m, 9H), 7.36 – 7.30 (m, 5H), 7.30 – 7.24 (m, 2H), 7.23 – 7.19 (m, 2H), 6.87 (d, *J* = 8.5 Hz, 2H), 1.28 (s, 18H). ^{13}C NMR (100 MHz, $CDCl_3$) δ 156.12, 144.77, 143.18, 141.67, 141.00, 139.63, 139.48, 134.44, 134.16, 131.26, 131.10, 130.38, 128.90, 128.76, 127.28, 127.01, 126.74, 126.71, 126.18, 124.85, 124.24, 123.11, 122.67, 121.96, 121.82, 120.50, 117.97, 117.73, 117.21, 34.36, 31.41. HRMS: (ESI) m/z calcd for $C_{74}H_{54}B_2N_2O_2$ $[M]^+$: 1024.4365; found: 1024.4405. Elemental analysis calcd. (%) for $C_{74}H_{54}B_2N_2O_2$: C, 86.72; H, 5.31; N, 2.73. Found: C, 86.56; H, 5.58; N, 2.60. Purity (HPLC): 99.71%.

Synthesis of 7-(2,5-dibromo-3,6-bis(4-(tert-butyl)phenoxy)-4-(3,6-diphenyl-9H-carbazol-9-yl)phenyl)-7H-dibenzo[c,g]carbazole (**5**)

Under argon atmosphere, compound **1** (2.8 g, 5 mmol), 3,6-diphenyl-9*H*-carbazole (1.6 g, 5 mmol), 7*H*-dibenzo[*c,g*]carbazole (1.3 g, 5 mmol) and Cs_2CO_3 (4.9 g, 15 mmol) were added into a two necked round bottom flask. Addition of DMF (30 mL) was added into the flask and the mixture was stirred for 12 hours at 80 °C. After cooling to room temperature, the mixture was poured into water and the crude product was obtained by filtration followed by washing with hot ethanol. Precursor **3** (2.2 g, 41%) was acquired as white solid. ^1H NMR (400 MHz, $CDCl_3$) δ 9.14 (d, *J* = 8.8 Hz, 2H), 8.24 (s, 2H), 8.04 (d, *J* = 8.0 Hz, 2H), 7.86 (d, *J* = 8.8 Hz, 2H), 7.79–7.63 (m, 8H), 7.59–7.45 (m, 6H), 7.43–7.32 (m, 4H), 7.31–7.17 (m, 2H), 6.75 (d, *J* = 8.8 Hz, 2H), 6.49 (d, *J* = 8.8 Hz, 2H), 6.20 (d, *J* = 8.4 Hz, 2H), 6.05 (d, *J* = 8.4 Hz, 2H), 0.95 (s, 9H), 0.64 (s, 9H). ^{13}C NMR (100 MHz, $CDCl_3$) δ 153.97, 153.76, 151.20, 150.70, 146.42, 146.26, 141.78, 139.05, 136.44, 134.19, 132.04, 131.32, 130.45, 129.20, 129.01, 128.86, 127.37, 126.75, 125.69, 125.51, 125.42, 125.35, 124.34, 123.65, 121.85, 121.50, 118.73, 118.42, 115.18, 115.10, 111.90, 110.97, 33.92, 33.59, 31.25, 30.76.

7,7'-(2,5-dibromo-3,6-bis(4-(tert-butyl)phenoxy)-1,4-phenylene)bis(7H-dibenzo[*c,g*]carbazole) (**6**)

The synthesis procedure of intermediate **6** is similar to that of compound **3**, employing compound **4** instead of compound **2**. Intermediate **6** (86%) was acquired as white solid. ^{1}H NMR (500 MHz, $CDCl_3$) δ 9.15 (d, *J* = 7.5 Hz, 4H), 8.05 (d, *J* = 7.5 Hz, 4H), 7.89 (d, *J* = 8.5 Hz, 4H), 7.69 (t, *J* = 7.5 Hz, 4H), 7.55 (t, *J* = 7.5 Hz, 4H), 7.39 (d, *J* = 8.5 Hz, 4H), 6.50 (d, *J* = 8.5 Hz, 4H), 6.06 (d, *J* = 7.5 Hz, 4H), 0.65 (s, 18H). Due to the poor solubility, the ^{13}C NMR spectra of compound **6** have not been offered.

*Synthesis of **PhBCzBN***

The synthesis procedure of **PhBCzBN** is similar to that of compound **PhCzBN**, employing compound **5** instead of compound **3**. Target product **PhBCzBN** (22%) was acquired as red solid. ^{1}H NMR (500 MHz, $CDCl_3$) δ 9.32 (d, *J* = 8.5 Hz, 1H), 9.24 (d, *J* = 8.5 Hz, 1H), 9.05 (s, 1H), 8.72 (d, *J* = 14.5 Hz, 2H), 8.57 (s, 1H), 8.42 (s, 1H), 8.24 (d, *J* = 8.0 Hz, 1H), 8.10 – 7.99 (m, 2H), 7.86–7.71 (m, 5H), 7.70–7.53 (m, 7H), 7.48–7.30 (m, 8H), 7.11 (d, *J* = 8.5 Hz, 1H), 7.03 (d, *J* = 8.5 Hz, 1H), 1.41 (s, 18H). ^{13}C NMR (100 MHz, $CDCl_3$) δ 156.27, 156.17, 145.16, 144.83, 143.01, 141.33, 140.94, 140.08, 139.73, 139.47, 139.43, 137.29, 135.88, 134.53, 134.50, 131.32, 131.25, 131.16, 131.07, 130.71, 130.56, 130.48, 130.17, 128.90, 128.84, 128.68, 128.66, 127.41, 127.13, 127.08, 126.79, 126.75, 126.74, 126.21, 125.83, 125.53, 125.16, 125.06, 124.96, 124.21, 123.77, 123.57, 123.31, 122.61, 121.44, 120.16, 118.30, 117.73, 117.70, 117.66, 117.50, 117.46, 117.43, 77.36, 77.04, 76.72, 34.43, 34.41, 31.48, 31.42. HRMS: (ESI) m/z calcd for $C_{70}H_{50}B_2N_2O_2$ $[M+H]^+$: 972.4053; found: 972.4053. Elemental analysis calcd. (%) for $C_{70}H_{50}B_2N_2O_2$: C, 86.43; H, 5.18; N, 2.88. Found: C, 86.21; H, 5.83; N, 2.74. Purity (HPLC): 99.82%.

*Synthesis of **BCzBN***

The synthesis procedure of **BCzBN** is similar to that of compound **PhCzBN**, employing compound **6** instead of compound **3**. Intermediate **BCzBN** (26%) was acquired as purplish red solid. ^{1}H NMR (400 MHz, $CDCl_3$) δ 9.15 (d, *J* = 8.4 Hz, 4H), 8.05 (d, *J* = 9.6 Hz, 4H), 7.89 (d, *J* = 8.8 Hz, 4H), 7.70 (d, *J* = 8.4 Hz, 1H), 7.55 (d, *J* = 7.2 Hz, 4H), 7.39 (d, *J* = 8.8 Hz, 4H), 6.50 (d, *J* = 8.8 Hz, 4H), 6.06 (d, *J* = 8.8 Hz, 4H), 1.54 (s, 18H). Due to the poor solubility, the ^{13}C NMR spectra have not been offered. HRMS: (ESI) m/z calcd for $C_{66}H_{46}B_2N_2O_2$ $[M+H]^+$: 920.3740; found: 920.3739. Elemental analysis calcd. (%) for $C_{66}H_{46}B_2N_2O_2$: C, 85.89; H, 5.04; N, 3.04. Found: C, 86.21; H, 5.73; N, 2.86. Purity (HPLC): 99.73%.

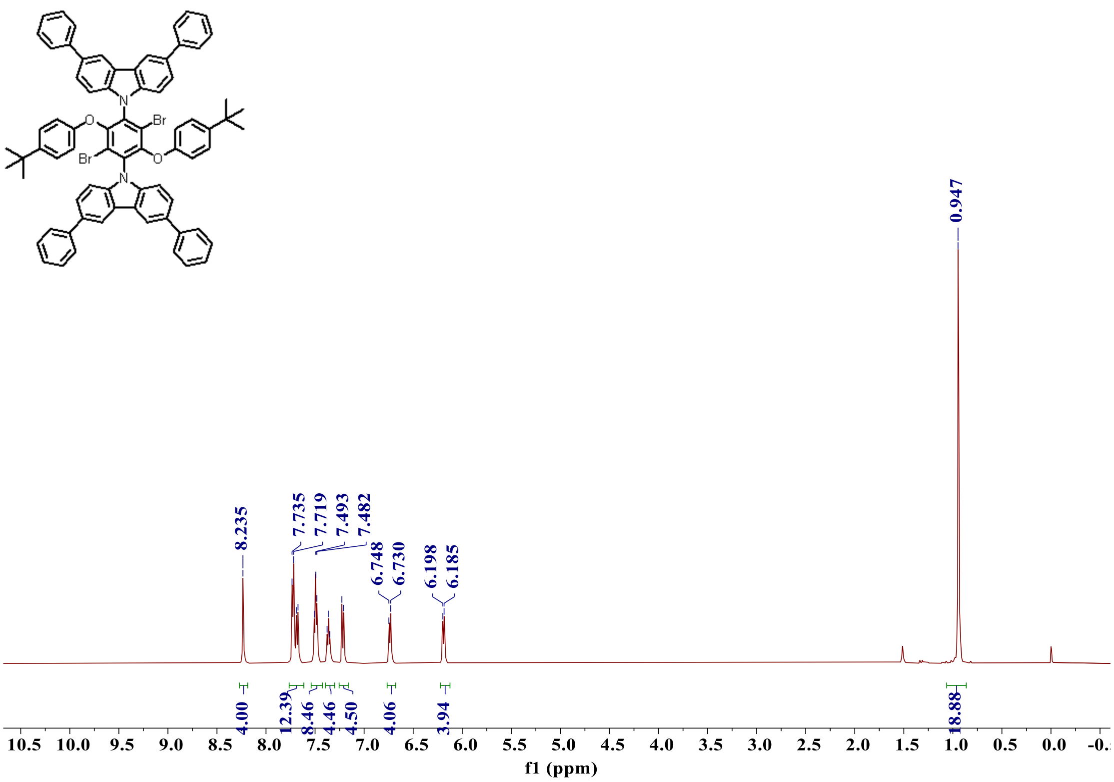

Figure S1. The ^{1}H NMR spectrum of compound **3**.

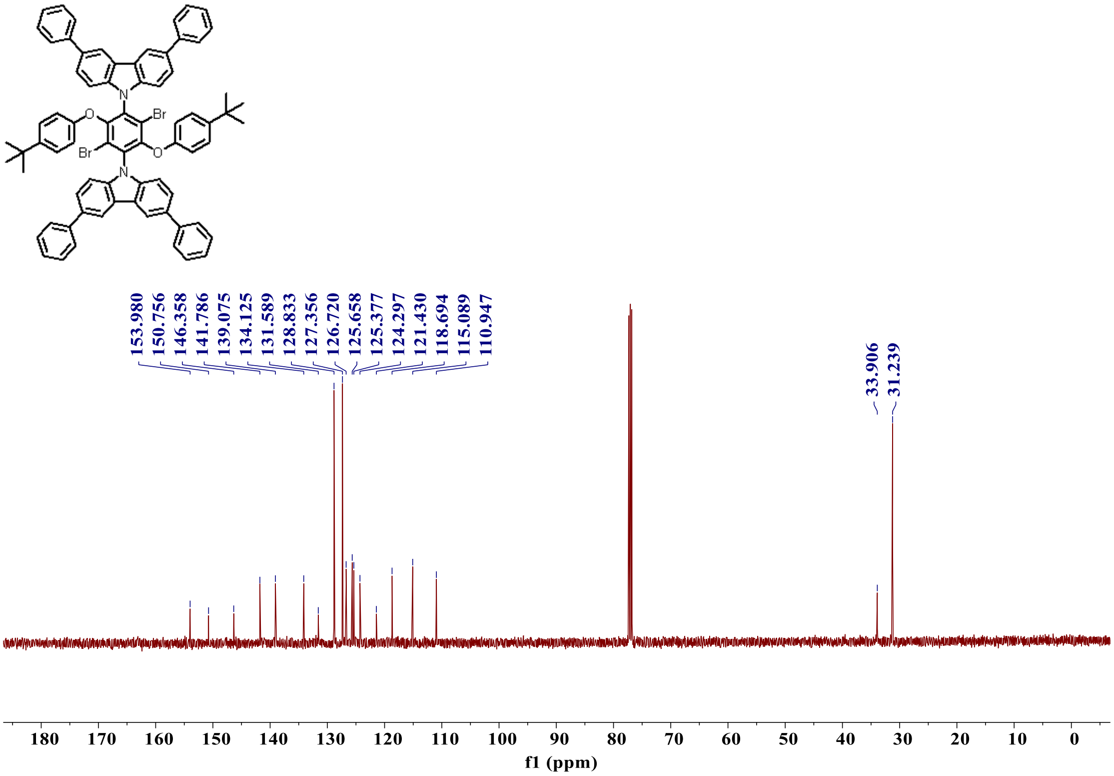

Figure S2. ^{13}C NMR spectrum of compound **3**.

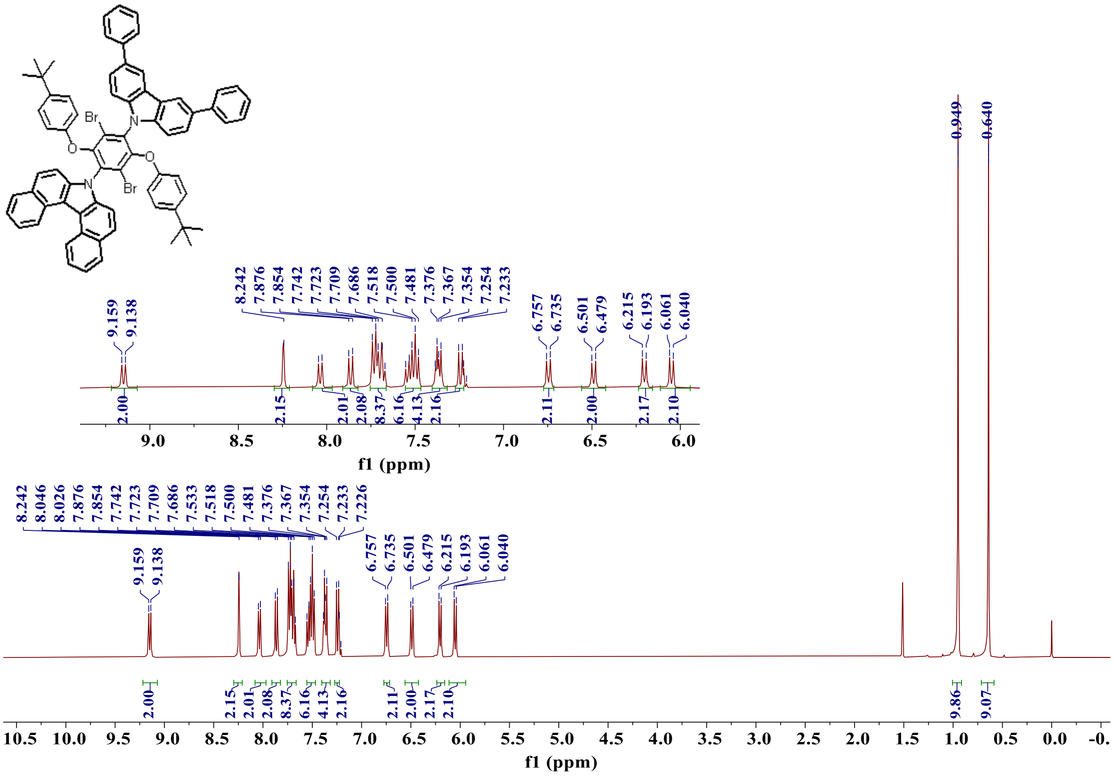

Figure S3. ^{1}H NMR spectrum of compound **5**.

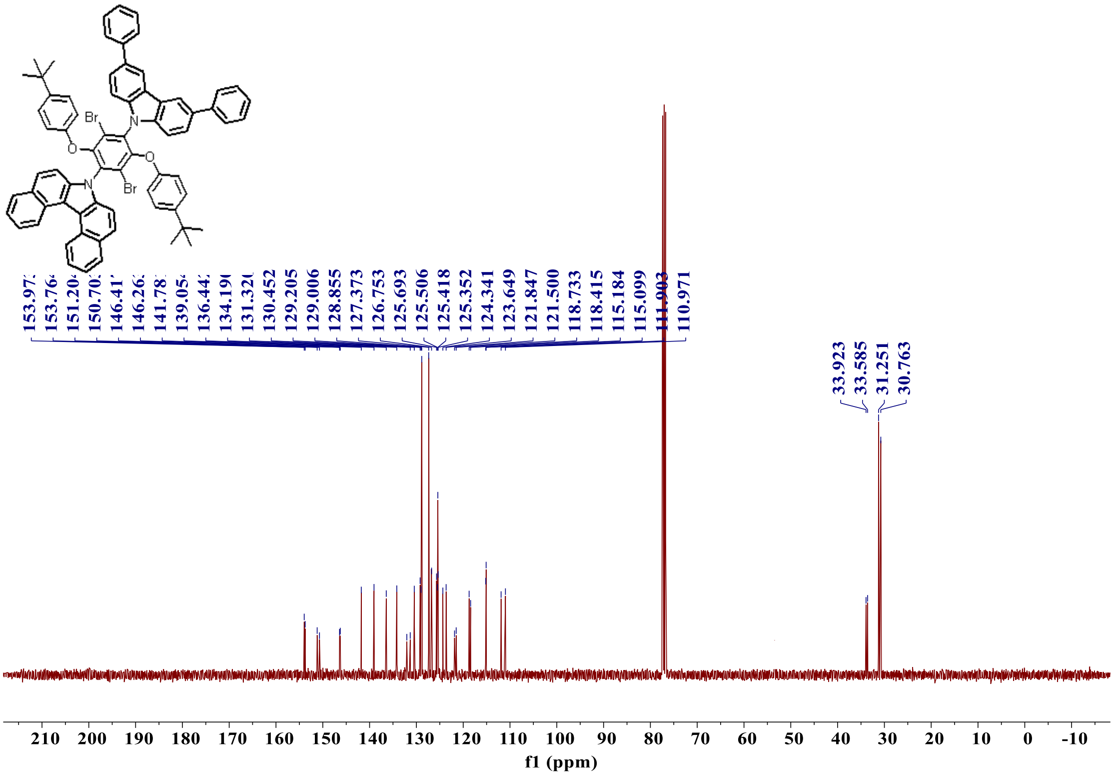

Figure S4. ^{13}C NMR spectrum of compound **5**.

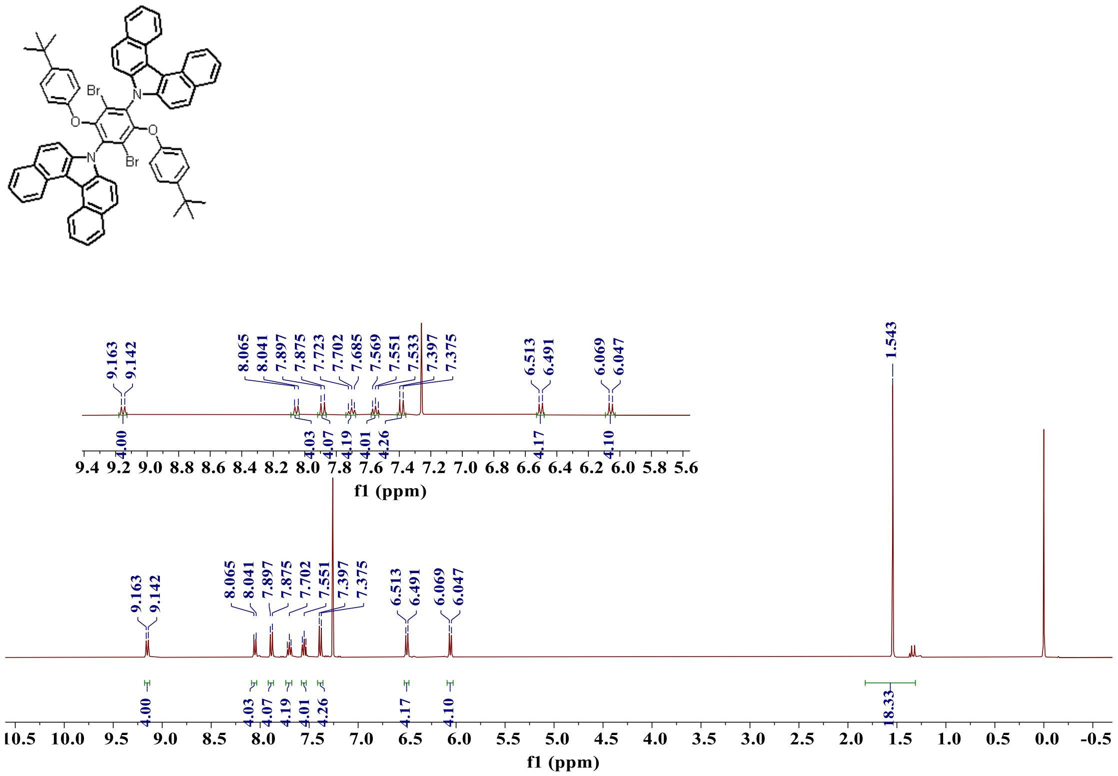

Figure S5. ^{1}H NMR spectrum of compound **7**.

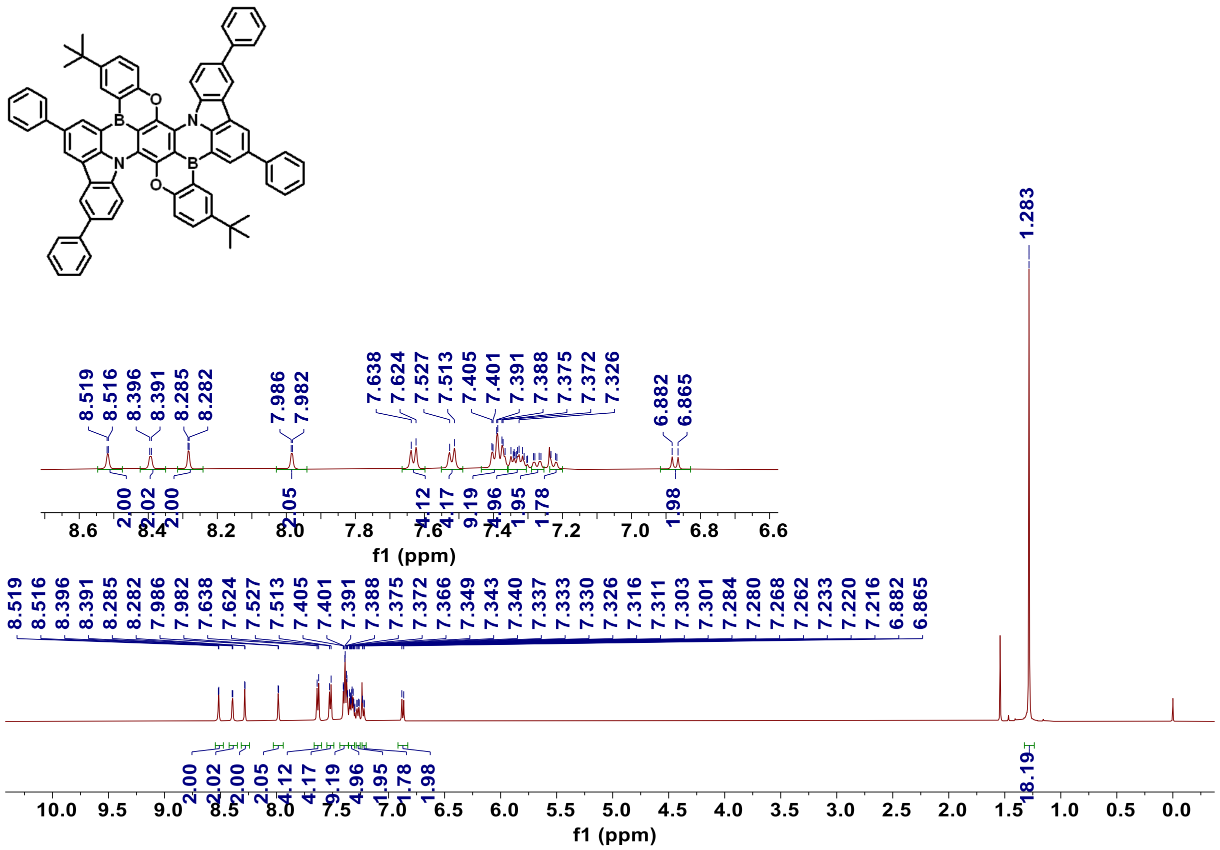

Figure S6. ^{1}H NMR spectrum of compound **PhCzBN**.

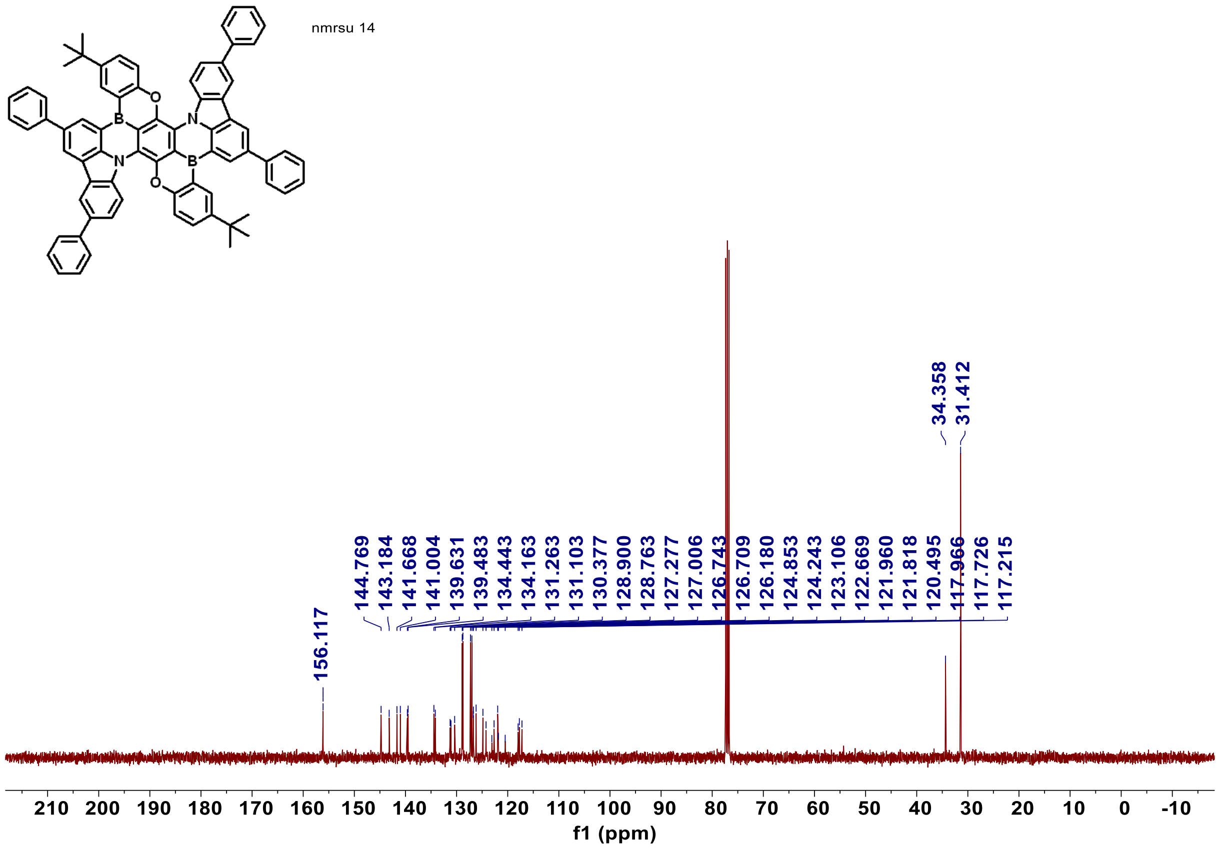

Figure S7. ^{13}C NMR spectrum of compound **PhCzBN**.

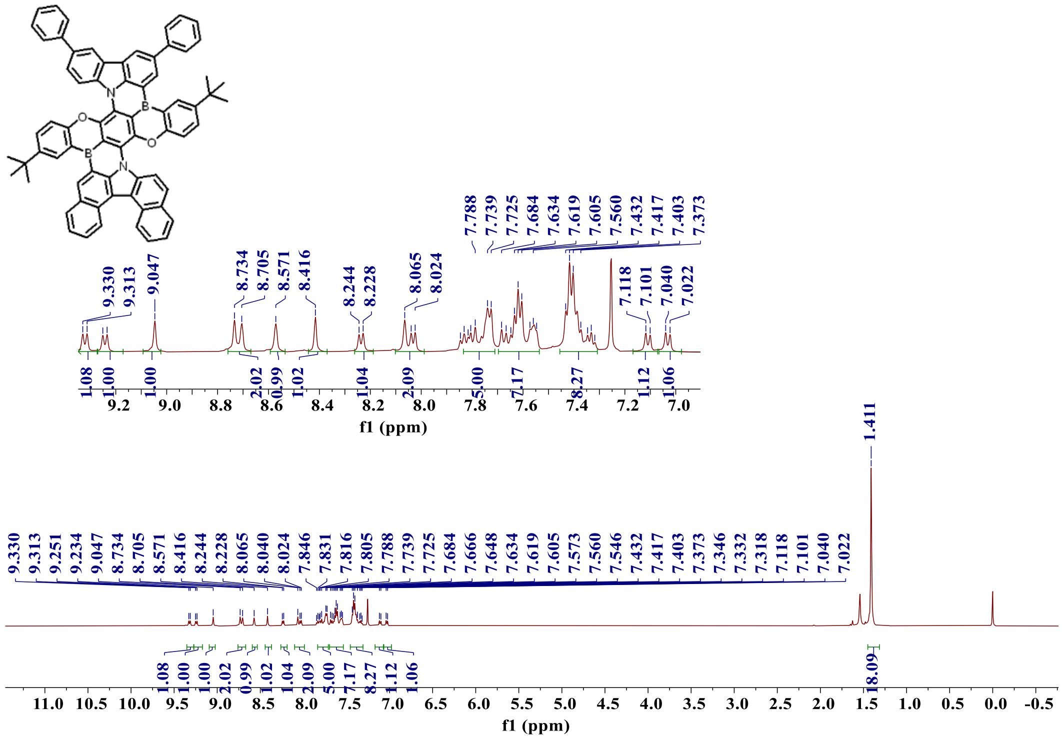

Figure S8. ^{1}H NMR spectrum of compound **PhBCzBN**.

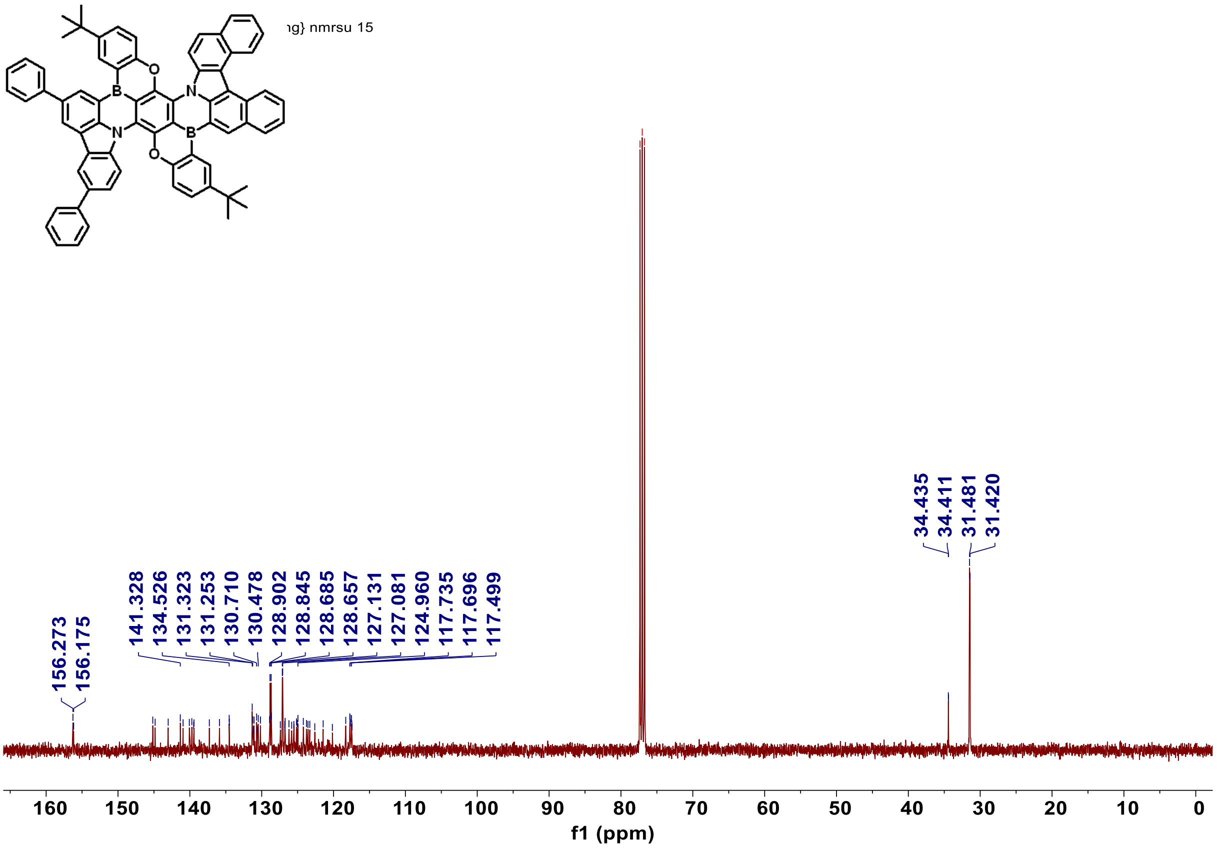

Figure S9. ^{13}C NMR spectrum of compound **PhBCzBN**.

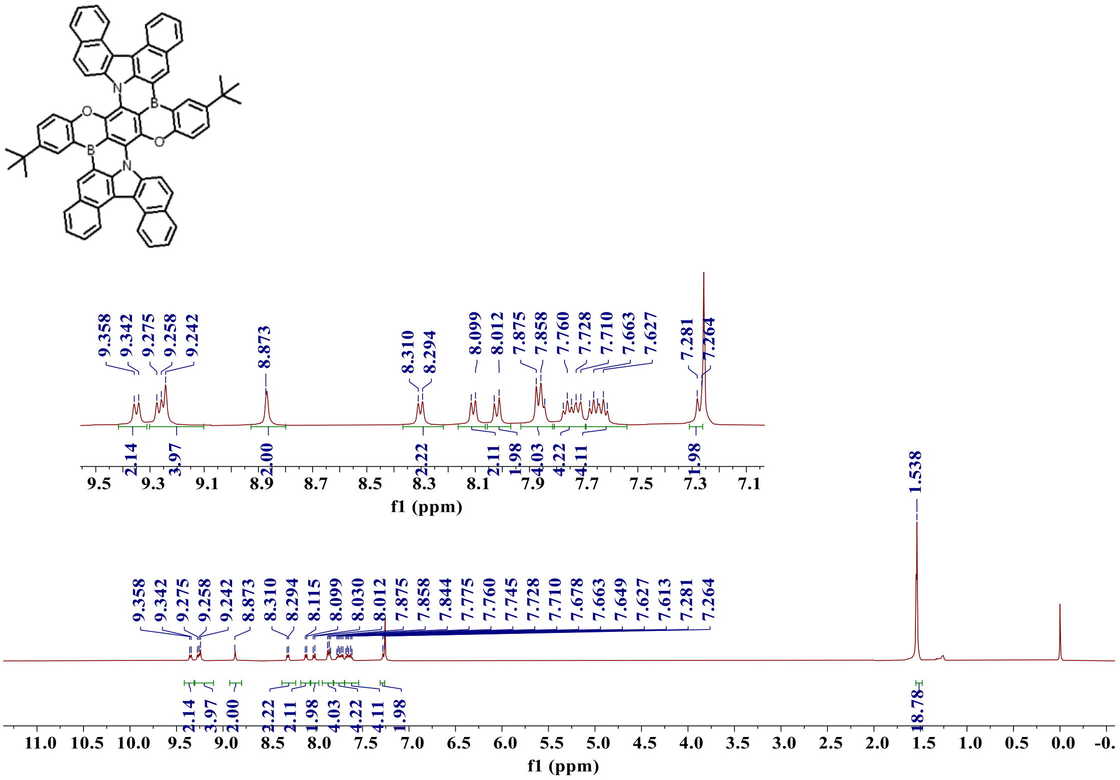

Figure S10. ^{1}H NMR spectrum of **BCzBN**.

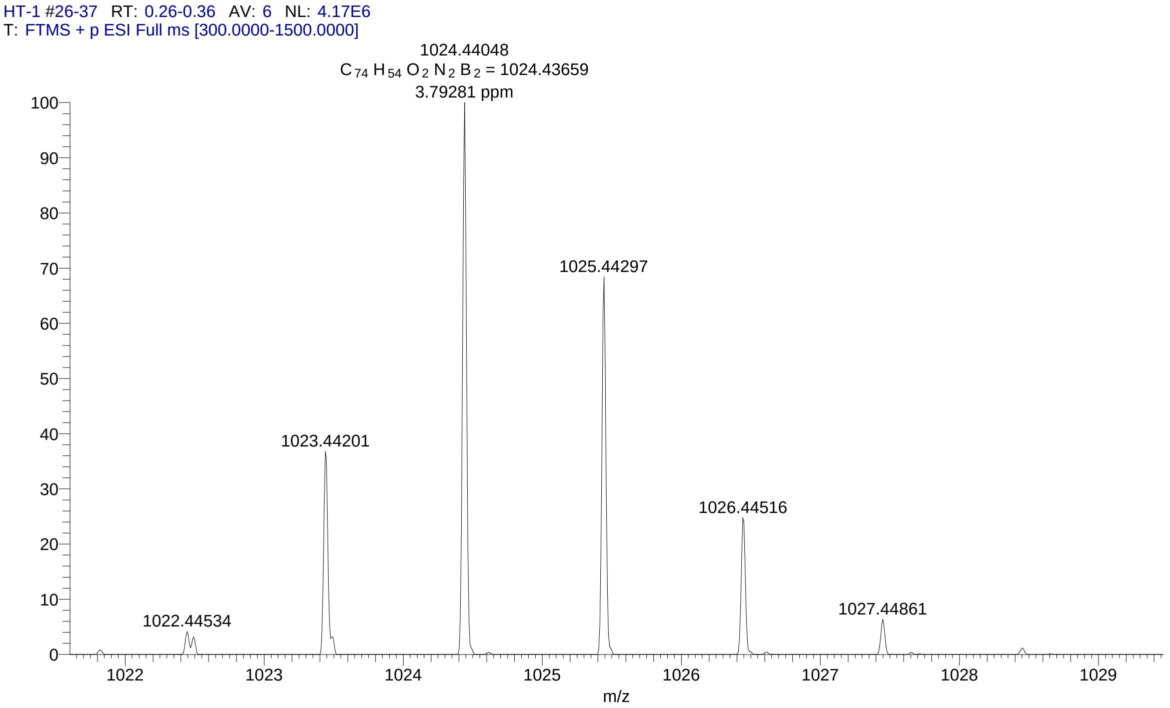

Figure S11. HR-MS spectrum of **PhCzBN**.

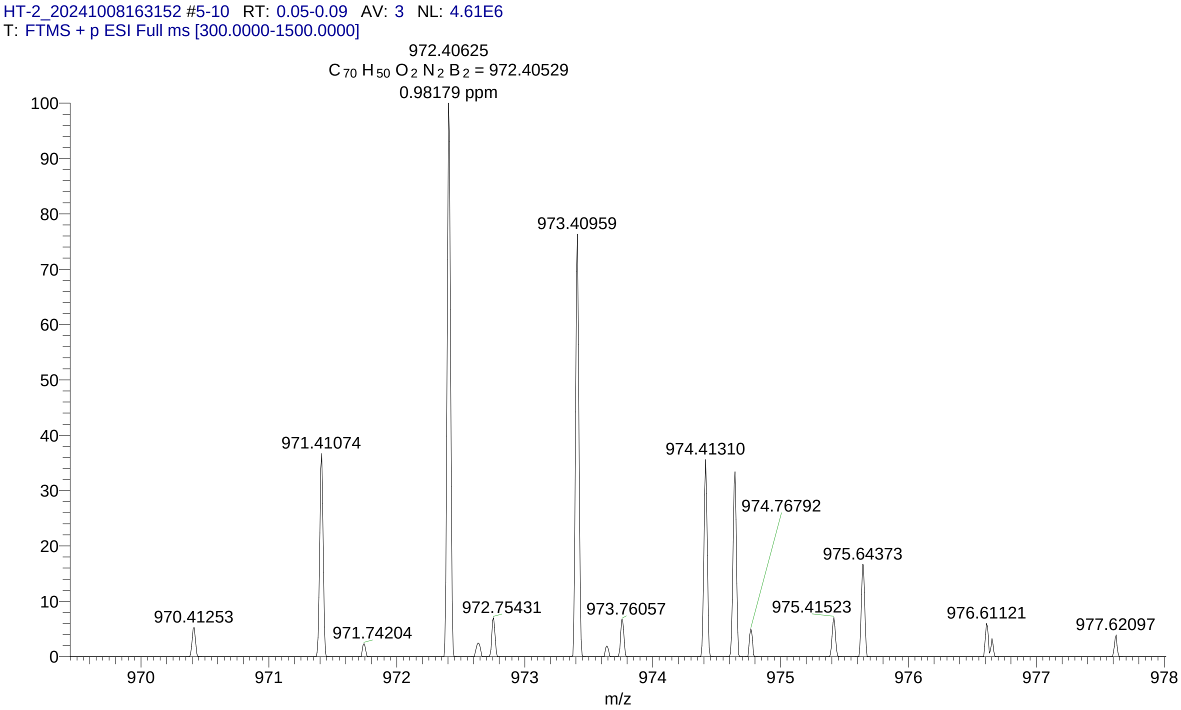

Figure S12. HR-MS spectrum of **PhBCzBN**.

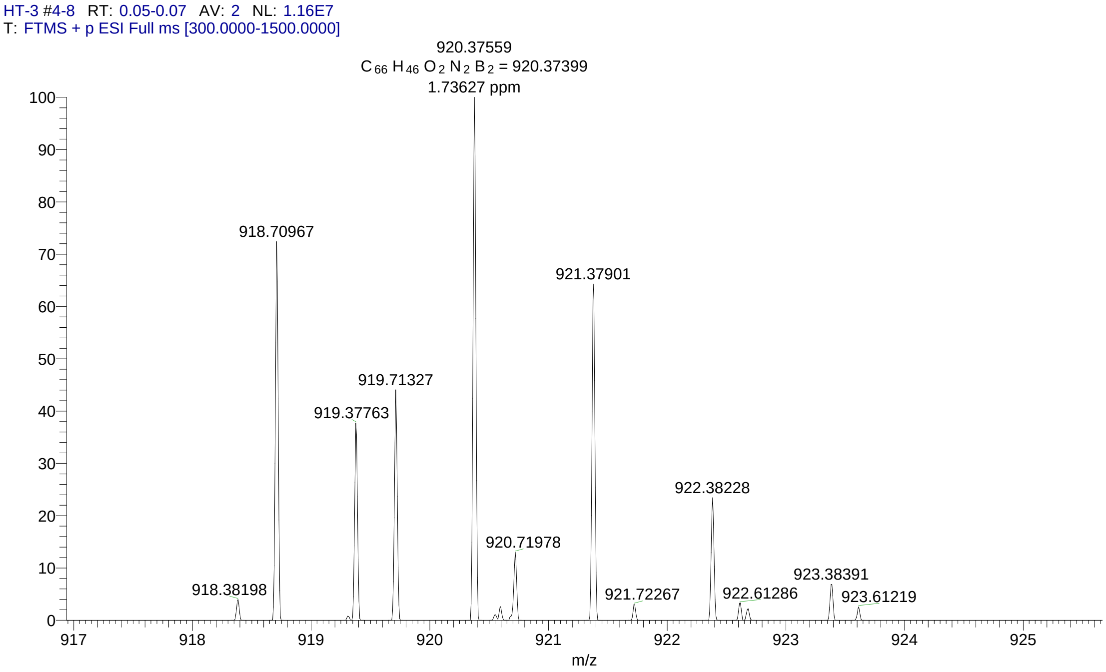

Figure S13. HR-MS spectrum of **BCzBN**.

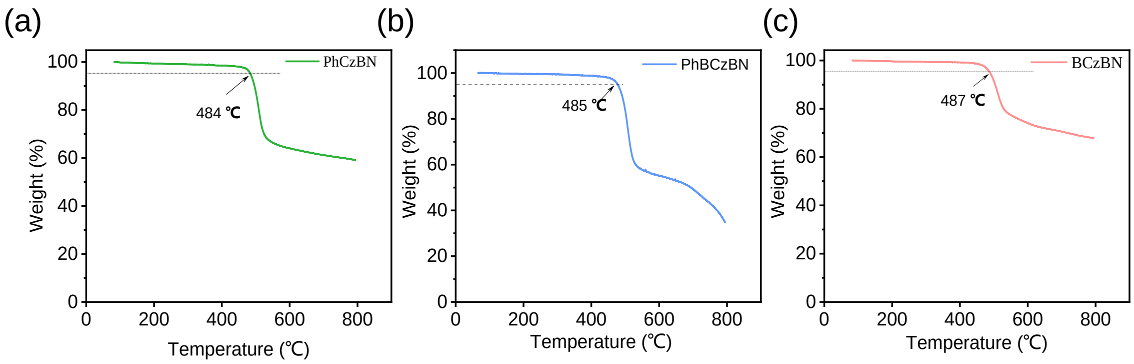

Figure S14. TGA curves of **PhCzBN**, **PhBCzBN** and **BCzBN**.

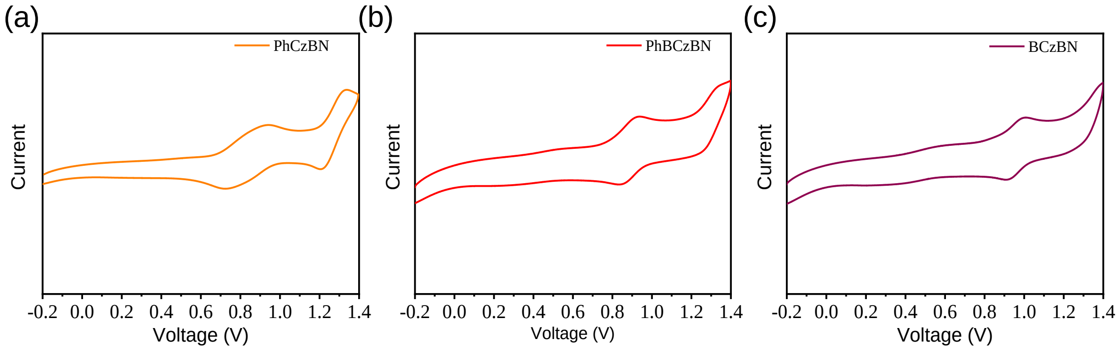

Figure S15. CV curves of **PhCzBN**, **PhBCzBN** and **BCzBN**.

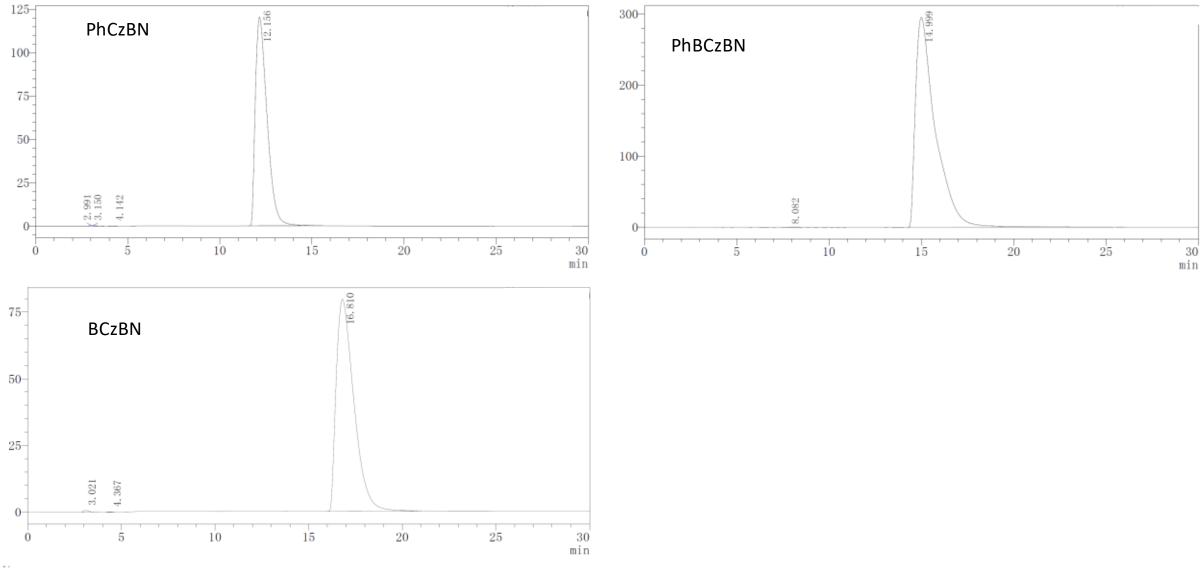

Figure S16. HPLC chromatogram of **PhCzBN**, **PhBCzBN**, and **BCzBN**.

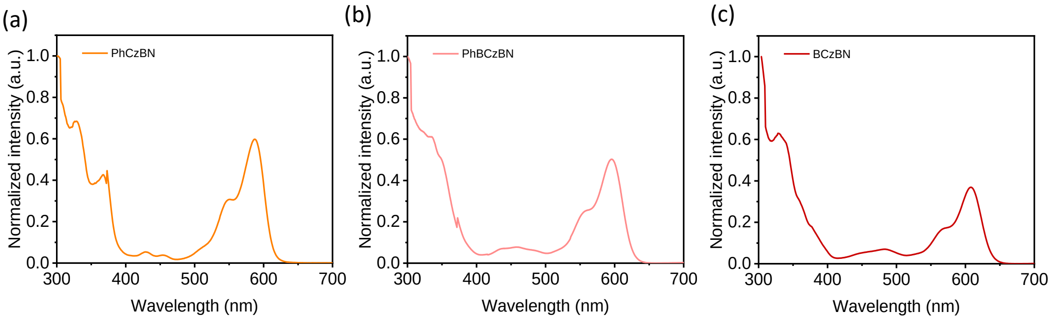

Figure S17. The UV-vis spectra of **PhCzBN**, **PhBCzBN**, and **BCzBN** in dilute toluene.

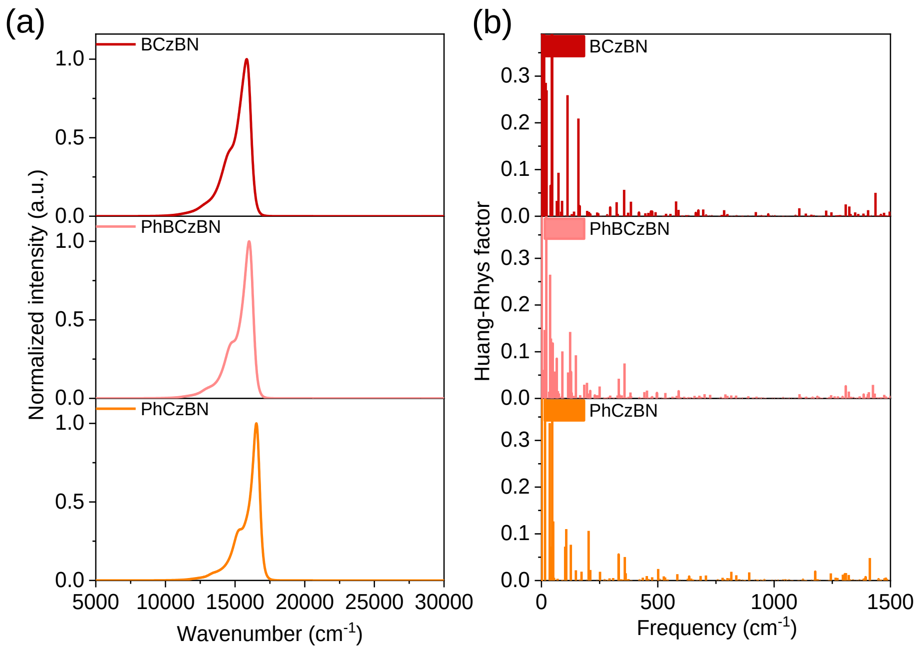

Figure S18. The calculated vibrationally resolved fluorescence spectra of PhCzBN, PhBCzBN, and BCzBN.

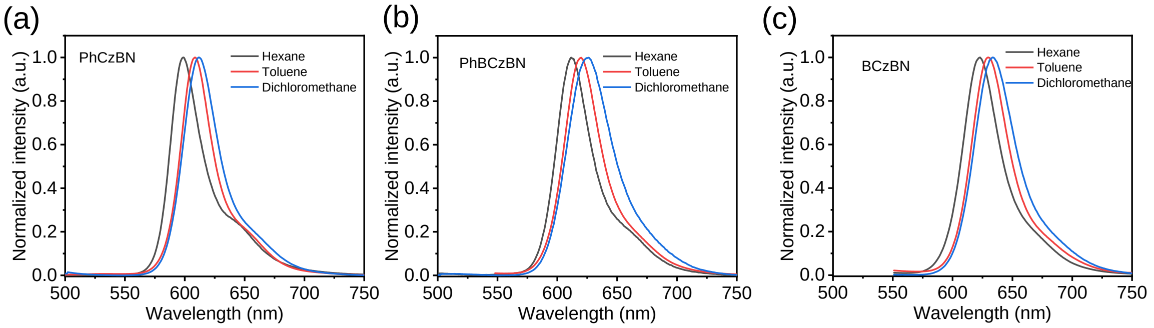

Figure S19. Fluorescence spectra of **PhCzBN**, **PhBCzBN** and **BCzBN** in different solvents at fixed concentration of 1.0×10^{-6} M.

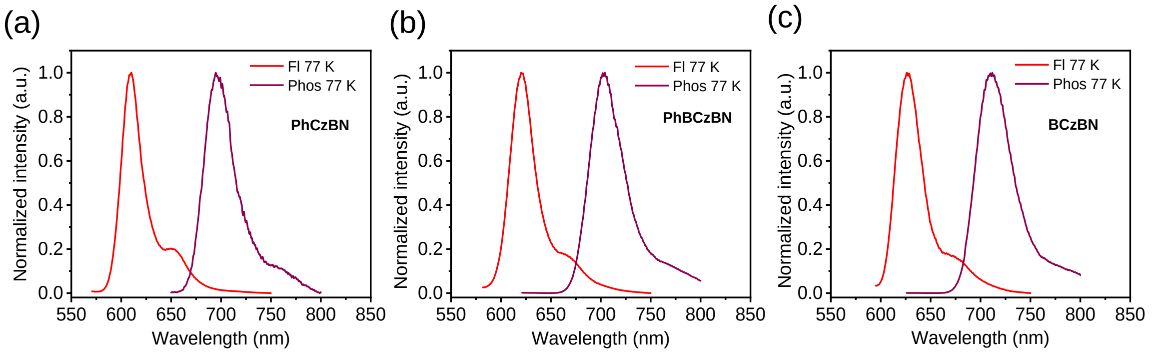

Figure S20. Fluorescence and phosphorescence spectra of **PhCzBN**, **PhBCzBN** and **BCzBN** at 77 K measured in dilute toluene solution.

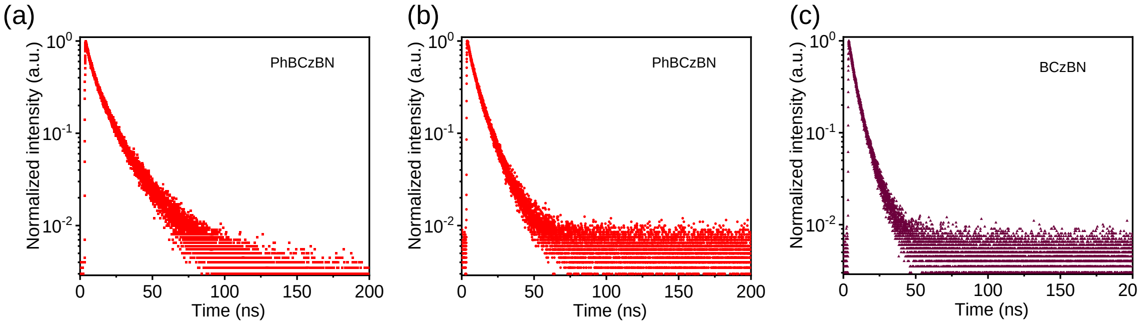

Figure S21. Transient photoluminescence curves (ns-scale) of **PhCzBN, PhBCzBN** and **BCzBN** at room temperature in the film state (1 wt% in DMIC-TRZ).

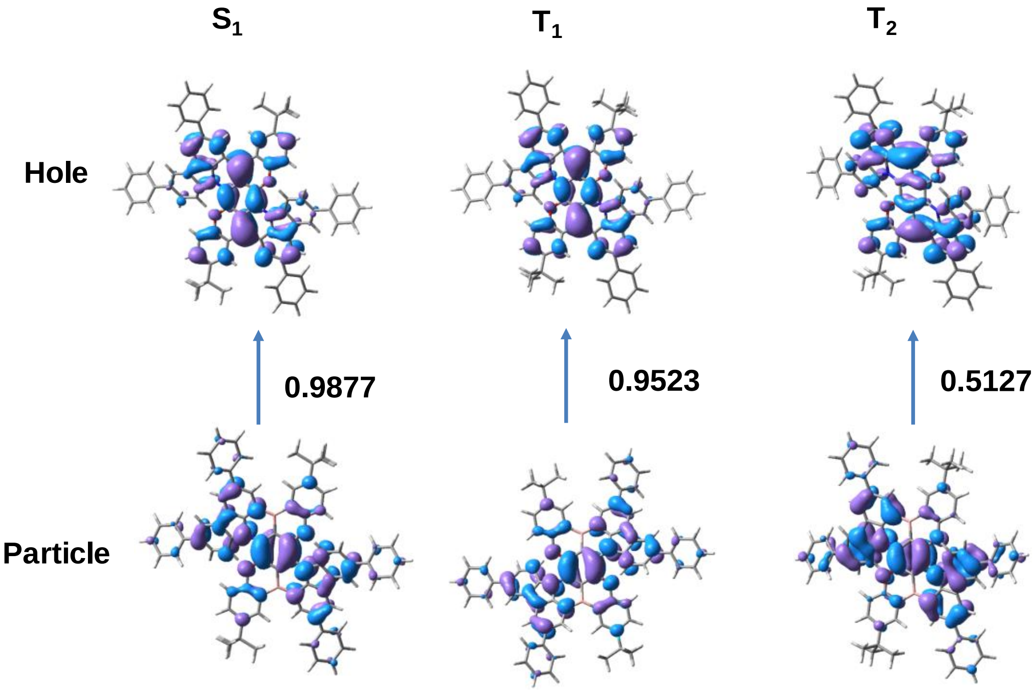

Figure S22. Highest occupied and lowest unoccupied natural transition orbitals (HONTOs and LUNTOs) for the T_2, T_1 and S_1 states of **PhCzBN**.

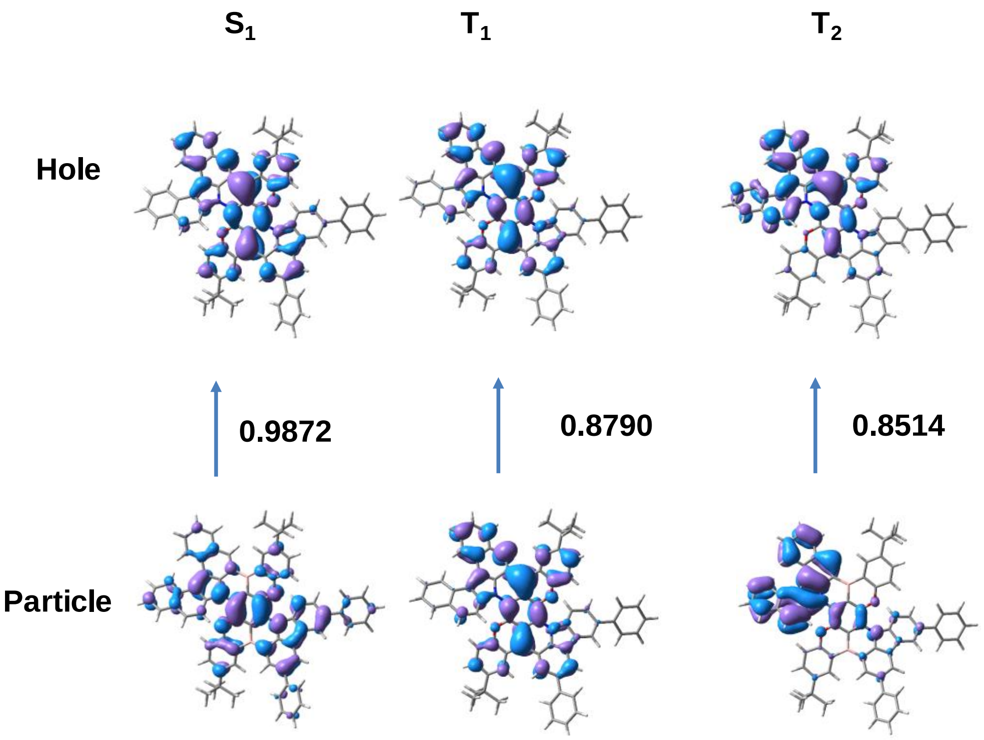

Figure S23. Highest occupied and lowest unoccupied natural transition orbitals (HONTOs and LUNTOs) for the T_2, T_1 and S_1 states of **PhBCzBN**.

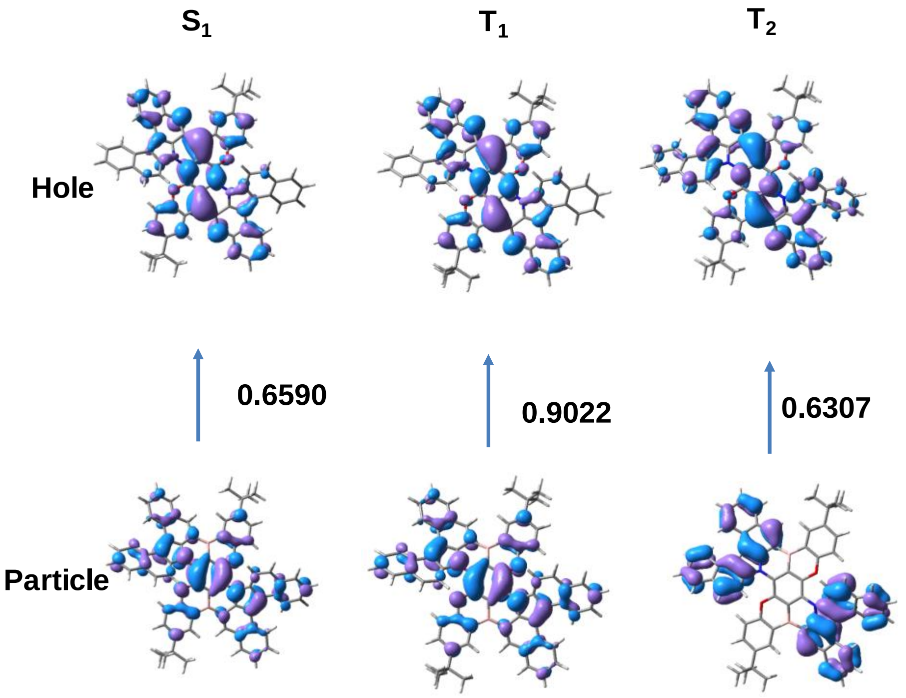

Figure S24. Highest occupied and lowest unoccupied natural transition orbitals (HONTOs and LUNTOs) for the T_2, T_1 and S_1 states of **BCzBN**.

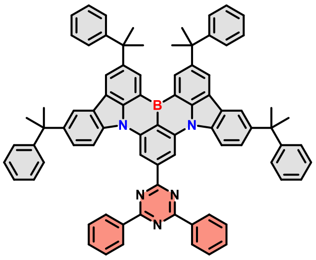

BN-R
λ = 624 nm, , FWHM = 46 nm
Angew. Chem. Int. Ed. 2022, *62*, e202216473

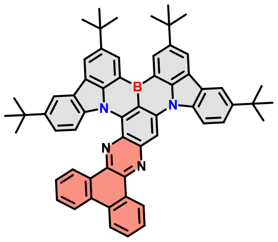

PPZ-BN
λ = 613 nm, FWHM = 48 nm
Angew. Chem. Int. Ed. 2023, *62*, e202300934

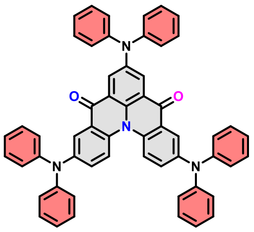

3TPA-DiKTa
λ = 617 nm, FWHM = 56 nm
Angew. Chem. Int. Ed. 2022, *61*, e202213697

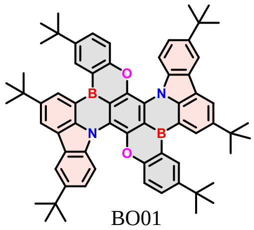

BO01
λ = 605 nm, FWHM = 32 nm
Adv. Mater. 2022, *34*, 2201442

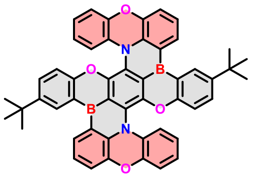

PXZBNO
λ = 627 nm, FWHM = 45 nm
Chem. Eng. J. 2023, *471*, 144565

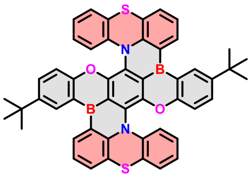

PTZBNO
λ = 612 nm, FWHM = 47 nm
Chem. Eng. J. 2023, *471*, 144565

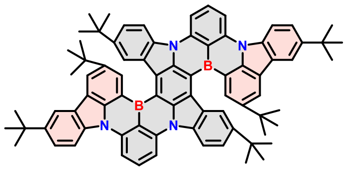

BBCz-R
λ = 615 nm, FWHM = 21 nm
J. Am. Chem. Soc. 2020, *142*, 19468

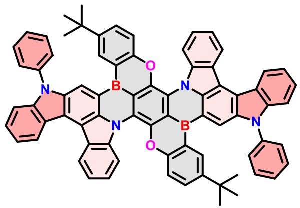

BNNO
λ = 637 nm, FWHM = 32 nm
Adv. Mater. 2023, *35*, 230101

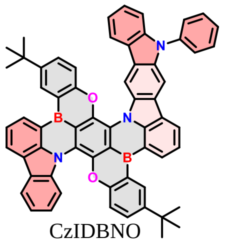

CzIDBNO
λ = 633 nm, FWHM = 38 nm
Sci. Adv. 2023, *9*, eadh8296

Figure S25. Chemical structure of classic red MR-TADF emitters and their photophysical performance.

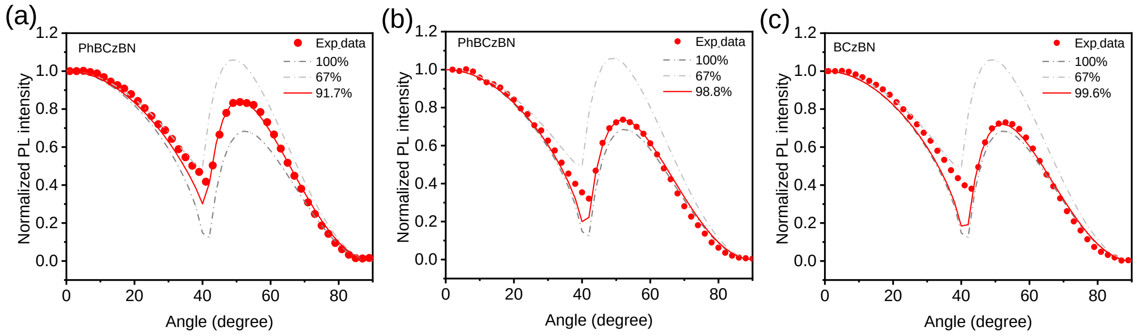

Figure S26. Angle-dependent *p*-polarized photoluminescence intensity and simulation curve for of **PhCzBN, PhBCzBN** and **BCzBN** at room temperature in the film state (1 wt% in DMIC-TRZ).

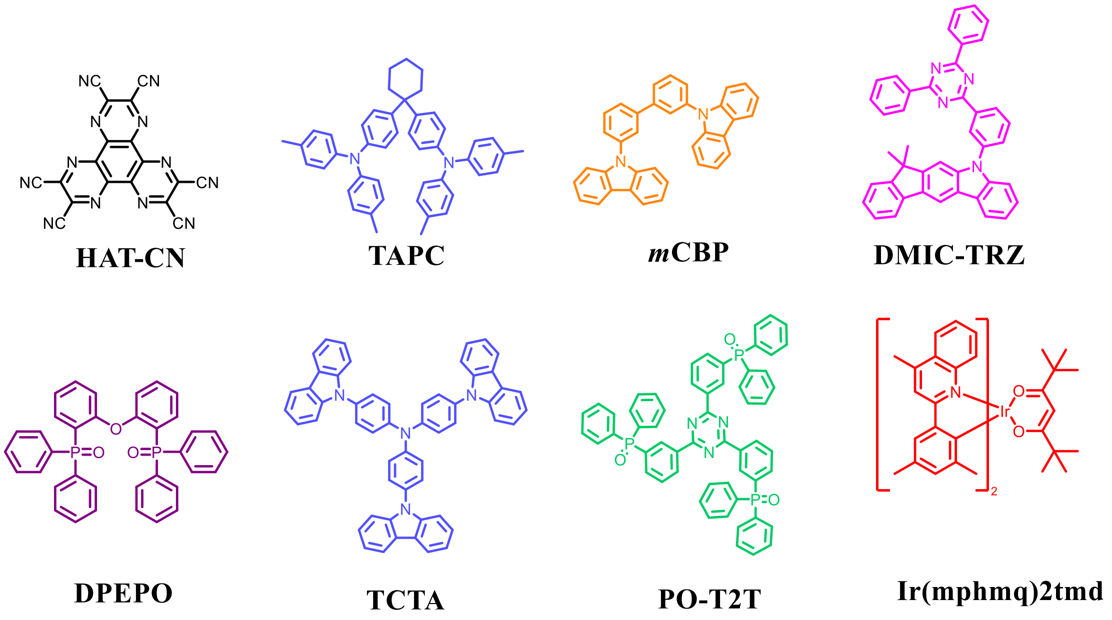

Figure S27. Chemical structures of the organic materials employed in the EL devices.

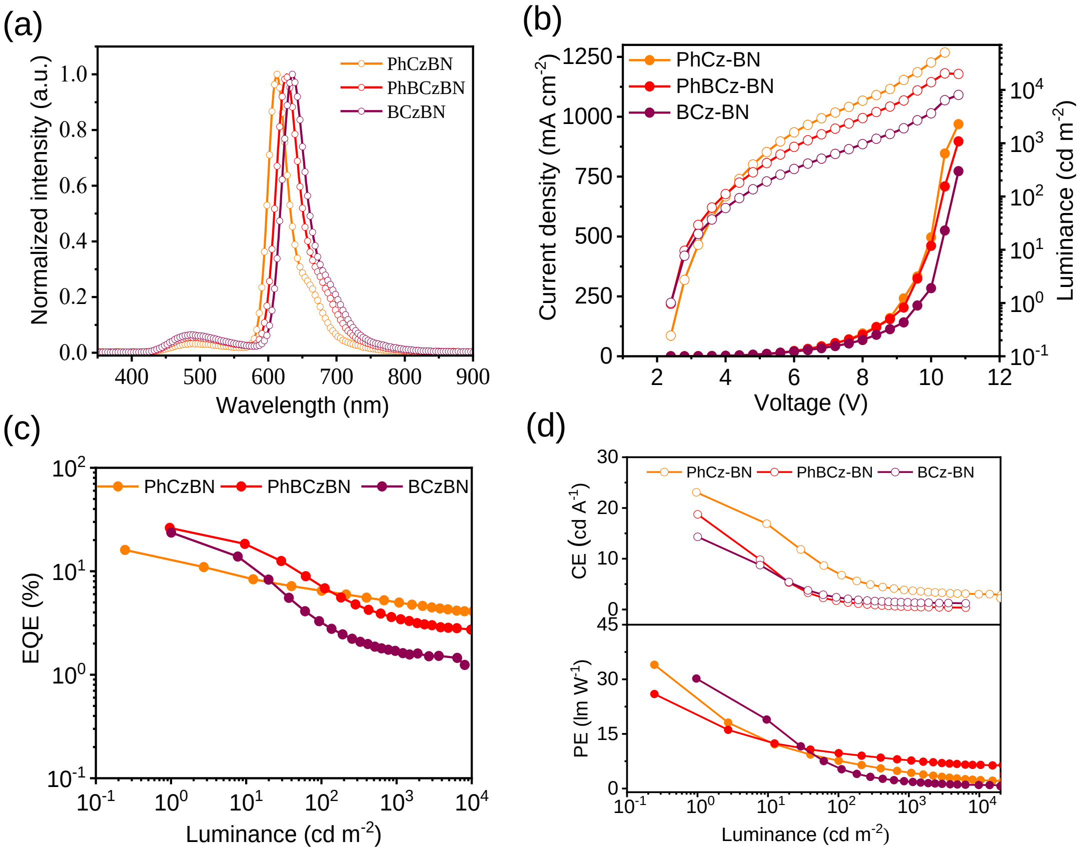

Figure S28. Electroluminescence properties of the non-sensitized devices based on **PhCzBN**, **PhBCzBN** and **BCzBN**.

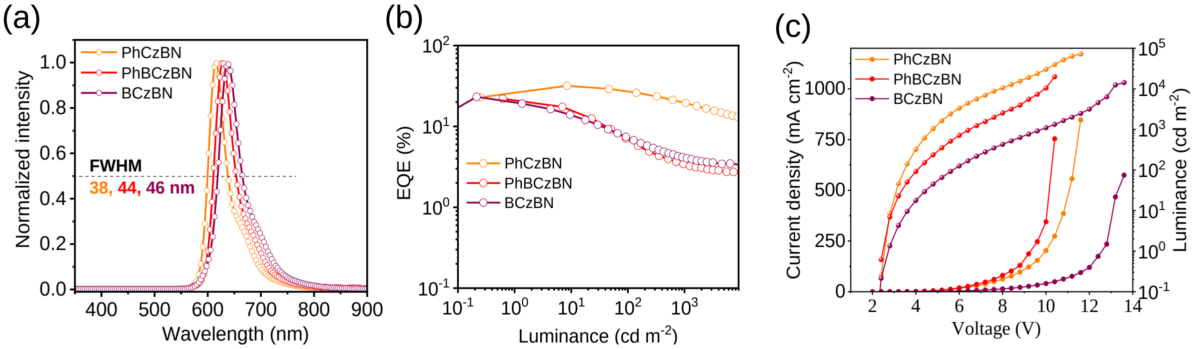

Figure S29. Electroluminescence properties of the sensitized devices based on **PhCzBN**, **PhBCzBN** and **BCzBN** at 2 wt% doping concentrations. a) EL spectra. b) EQE versus luminance curves. c) Current density and luminance versus voltage curves.

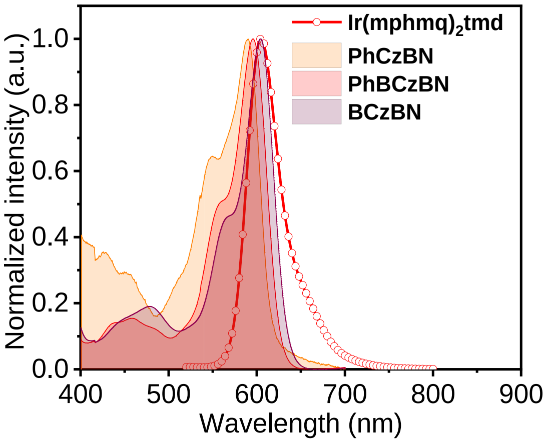

Figure S30. The absorption spectra of **PhCzBN**, **PhBCzBN**, and **BCzBN** as well as the emission spectrum of sensitizer Ir(mphmq)$_2$tmd in toluene.

Table S1 Crystal data and structure refinement for **BCzBN (**Deposition Number: 2373696**)**.

Empirical formula	$C_{66}H_{46}B_2N_2O_2$
Formula weight	920.67
Temperature/K	170.00
Crystal system	trigonal
Space group	R-3
a/Å	41.575(3)
b/Å	41.575(3)
c/Å	17.6054(18)
α/°	90
β/°	90
γ/°	120
Volume/Å^3	26354(5)
Z	18
ρ_{calc}g/cm^3	1.044
μ/mm^{-1}	0.304
F(000)	8676.0
Crystal size/mm^3	0.35 × 0.03 × 0.02
Radiation	GaKα (λ = 1.34139)
2Θ range for data collection/°	4.86 to 114.056
Index ranges	$-49 \le h \le 35$, $-51 \le k \le 51$, $-22 \le l \le 16$
Reflections collected	67582
Independent reflections	11934 [R_{int} = 0.1625, R_{sigma} = 0.1517]
Data/restraints/parameters	11934/0/655
Goodness-of-fit on F^2	0.965
Final R indexes [I>=2σ (I)]	R_1 = 0.0881, wR_2 = 0.2167
Final R indexes [all data]	R_1 = 0.1575, wR_2 = 0.2650
Largest diff. peak/hole / e Å^{-3}	0.45/-0.44

Table S2. Key data of the pure-red TSF-OLEDs at 2 wt% doping concentrations.

Emitter	V_{on} [V]	λ_{EL} [nm]	L_{max} [cd m^{-2}]	CE_{max} [cd A^{-1}]	PE_{max} [lm W^{-1}]	EQE [%] max/100/1000	FWHM [nm/eV]	CIE [x, y]
PhCzBN	2.6	615	72028	40.7	46.6	30.9/26.7/19.0	39/0.13	(0.668.0.332)
PhBCzBN	2.6	627	19930	20.0	26.1	22.0/7.1/3.4	44/0.14	(0.674, 0.320)
BCzBN	2.6	639	14295	13.0	17.0	23.3/7.1/4.1	45/0.15	(0.693, 0.306)

Table S3. The EL performance of representative red OLEDs with CIE$_x$ beyond 0.66.

Emitter	λ_{EL} (nm)	EQE (%)	CE_{max} (cd A^{-1})	CIE (x,y)	FWHM (nm)	Reference
PT-TPA	632	29.7	30.0	(0.66, 0.34)	NA	[2]
TPA–PZCN	628	28.1	20.0	(0.66, 0.34)	NA	[3]
PPZ-BN	613	26.9	34.5	(0.66, 0.34)	55	[4]
TPA-CN-N4	670	20.0	9.6	(0.68, 0.32)	NA	[5]
PCNQ-TPA	660	30.3	13.4	(0.69, 0.31)	NA	[6]
BCN-TPA	656	27.6	13.4	(0.686, 0.304)	NA	[7]
SOIrOPh	640	25.8	12.8	(0.68, 0.30)	NA	[8]
SOIrB1	636	19.0	19.6	(0.68, 0.31)	NA	
SOIrB2	644	18.5	9.07	(0.69, 0.31)	NA	
Ir(4tfmpq)$_2$mND	628	30.1	25.6	(0.67, 0.33)	NA	[9]
Ir(4tfmpq)$_2$mmND	628	31.5	25.2	(0.67, 0.33)	NA	
Ir(4tfmpq)$_2$mpND	620	27.7	27.0	(0.66, 0.34)	NA	
1F-Ir	622	26.8	23.8	(0.66, 0.33)	NA	[10]
Ir(A2)(L2)	613	24.3	23.7	(0.66, 0.34)	NA	[11]
ICzqz-Ir	618	17.8	28.8	(0.66, 0.34)	43	[12]
BNO3	625	36.1	43.4	(0.66, 0.34)	40	[13]
BBCz-R	616	22.0	NA	(0.67, 0.33)	26	[14]
PXZBNO	632	28.1	25.1	(0.67, 0.33)	54	[15]
PTZBNO	637	22.5	16.7	(0.69, 0.31)	54	
CzIDBNO	643	32.5	20.2	(0.701, 0.298)	47	[16]
IDIDBNO	671	27.2	8.4	(0.702, 0.297)	49	
BN-R	618	20.1	25.5	(0.663, 0.337)	47	[17]
BNNO	643	34.4	25.2	(0.708, 0.292)	42	[18]
PhCzBN	614	31.5	42.5	(0.674, 0.336)	40	**This work**

PhBCzBN	626	33.6	30.5	(0.682, 0.317)	44	
BCzBN	636	33.8	27.7	(0.700, 0.300)	44	

References

[1] M. Kállay, P. R. Nagy, D. Mester, Z. Rolik, G. Samu, J. Csontos, J. Csóka, P. B. Szabó, L. Gyevi-Nagy, B. Hégely, I. Ladjánszki, L. Szegedy, B. Ladóczki, K. Petrov, M. Farkas, P. D. Mezei, Á. Ganyecz, *J. Chem. Phys.* 2020, **152**, 074107.

[2] Y.-Y. Wang, K.-N. Tong, K. Zhang, C.-H. Lu, X. Chen, J.-X. Liang, C.-K. Wang, C.-C. Wu, M.-K. Fung, J. Fan, *Mater. Horiz.* 2021, **8**, 1297-1303.

[3] Y. L. Zhang, Q. Ran, Q. Wang, Y. Liu, C. Hänisch, S. Reineke, J. Fan, L. S. Liao, *Adv. Mater.* 2019, *31*, 1902368.

[4] H. Chen, T. Fan, G. Zhao, D. Zhang, G. Li, W. Jiang, L. Duan, Y. Zhang, *Angew. Chem. Int. Ed.* 2023, **35,** e202300934.

[5] J.-L. He, Y. Tang, K. Zhang, Y. Zhao, Y.-C. Lin, C.-K. Hsu, C.-H. Chen, T.-L. Chiu, J.-H. Lee, C.-K. Wang, C.-C. Wu, J. Fan, *Mater. Horiz.* 2022, **9,** 772-779.

[6] Z. Li, D. Yang, C. Han, B. Zhao, H. Wang, Y. Man, P. Ma, P. Chang, D. Ma, H. Xu, *Angew. Chem. Int. Ed.* 2021, **60,** 14846-14851.

[7] H. Wang, J.-X. Chen, X.-C. Fan, Y.-C. Cheng, L. Zhou, X. Zhang, J. Yu, K. Wang, X.-H. Zhang, *ACS Appl. Mater. Interfaces* 2022, **15,** 1685-1692.

[8] Y. Sun, X. Yang, Z. Feng, B. Liu, D. Zhong, J. Zhang, G. Zhou, Z. Wu, *ACS Appl. Mater. Interfaces* 2019, **11,** 26152-26164.

[9] G.-Z. Lu, Q. Zhu, L. Liu, Z.-G. Wu, Y.-X. Zheng, L. Zhou, J.-L. Zuo, H. Zhang, *ACS Appl. Mater. Interfaces* 2019, **11,** 20192-20199.

[10] B. Liang, Z. Yu, X. Zhuang, J. Wang, J. Wei, K. Ye, Z. Zhang, Y. Liu, Y. Wang, *Chem. Eur. J.* 2020, **26,** 4410-4418.

[11] P. Gnanasekaran, Y. Yuan, C.-S. Lee, X. Zhou, A. K. Y. Jen, Y. Chi, *Inorg. Chem.* 2019, **58,** 10944-10954.

[12] Z. P. Yan, M. X. Mao, Q. M. Liu, L. Yuan, X. F. Luo, X. J. Liao, W. Cai, Y. X. Zheng, *Adv. Funct. Mater.* 2024, **34,** 2402906.

[13] Y. Zou, J. Hu, M. Yu, J. Miao, Z. Xie, Y. Qiu, X. Cao, C. Yang, *Adv. Mater.* 2022, **34,** 2201442.

[14] M. Yang, I. S. Park, T. Yasuda, *J. Am. Chem. Soc.* 2020, **142,** 19468-19472.

[15] J. He, Y. Xu, S. Luo, J. Miao, X. Cao, Y. Zou, *Chem. Eng. J.* 2023, **471,** 144565.

[16] Y. Y. Jing, N. Q. Li, X. S. Cao, H. Wu, J. S. Miao, Z. X. Chen, M. L. Huang, X. Z. Wang, Y. X. Hu, Y. Zou, C. L. Yang, *Sci. Adv.* 2023, **9,** eadh8296.

[17] X. L. Cai, Y. C. Xu, Y. Pan, L. J. Li, Y. X. Pu, X. M. Zhuang, C. L. Li, Y. Wang, *Angew. Chem. Int. Ed.* 2023, **62,** e202216473.

[18] T. J. Fan, M. X. Du, X. Q. Jia, L. Wang, Z. Yin, Y. L. Shu, Y. W. Zhang, J. B. Wei, D. D. Zhang, L. Duan, *Adv. Mater.* 2023, **35,** e2301018.